

## Article

# Metal Fragments of Roman Pipes from Pompeii: Investigations on Copper-Based Alloys, Corrosion Products, and Surface Treatments

Sofia Schiattone <sup>1</sup>, Carla Martini <sup>2</sup>, Marco Malagodi <sup>3</sup>, Giacomo Fiocco <sup>3,4</sup>, Eleonora Rocconi <sup>3</sup>, Maria Morisco <sup>5</sup> and Cristina Chiavari <sup>1,\*</sup>

<sup>1</sup> Department of Cultural Heritage, University of Bologna, Via degli Ariani 1, 48121 Ravenna, Italy; sofia.schiattone@unibo.it

<sup>2</sup> Department of Industrial Engineering, University of Bologna, Viale Risorgimento 4, 40136 Bologna, Italy; carla.martini@unibo.it

<sup>3</sup> Department of Musicology and Cultural Heritage, University of Pavia, Corso Garibaldi 178, 26100 Cremona, Italy; marco.malagodi@unipv.it (M.M.); giacomo.fiocco@unipv.it (G.F.); eleonora.rocconi@unipv.it (E.R.)

<sup>4</sup> Arvedi Laboratory of Non-Invasive Diagnostics, CISRiC, University of Pavia, Via Bell'Aspa 3, 26100 Cremona, Italy

<sup>5</sup> Museo Archeologico Nazionale di Napoli, 80135 Napoli, Italy; maria.morisco@cultura.gov.it

\* Correspondence: cristina.chiavari@unibo.it

**Abstract:** This work reports the study of metal fragments from Roman pipes excavated from the archaeological site of Pompeii and currently preserved in the deposits of the National Archaeological Museum of Naples (MANN). The Roman pipe, called the *tibia*, is a reed wind musical instrument similar to the Greek *aulos*. It can be made of wood, bone, and/or metal. Materials consisting of metal Cu-based alloys were excavated from archaeological burial environments. This research aims to identify the composition of the alloys, characterize the corrosion patinas, and identify any ancient surface treatments on the fragments. Non-invasive and micro-invasive techniques were used to achieve this aim, i.e., optical microscopy, Raman spectroscopy, attenuated total reflectance Fourier-transform infrared spectrophotometry, scanning electron microscopy, and energy dispersive spectrometry. This research contributes to a deeper understanding of the materials and manufacturing techniques used for these instruments, as well as the degradation processes occurring over the centuries.

**Keywords:** Roman pipes; metal fragments; corrosion patinas; archeological burial environment; optical microscopy; Raman spectroscopy; FTIR; SEM/EDS



**Citation:** Schiattone, S.; Martini, C.; Malagodi, M.; Fiocco, G.; Rocconi, E.; Morisco, M.; Chiavari, C. Metal Fragments of Roman Pipes from Pompeii: Investigations on Copper-Based Alloys, Corrosion Products, and Surface Treatments. *Heritage* **2024**, *7*, 2538–2551. <https://doi.org/10.3390/heritage7050121>

Academic Editor: Nick Schiavon

Received: 11 April 2024

Revised: 6 May 2024

Accepted: 9 May 2024

Published: 14 May 2024



**Copyright:** © 2024 by the authors. Licensee MDPI, Basel, Switzerland. This article is an open access article distributed under the terms and conditions of the Creative Commons Attribution (CC BY) license (<https://creativecommons.org/licenses/by/4.0/>).

## 1. Introduction

This research was carried out as part of a scientific project whose aim is to study, conserve, restore, and promote a largely forgotten yet valuable collection of ancient Roman musical instruments excavated in Pompeii in the 18th and 19th centuries and currently kept in the National Archaeological Museum of Naples (MANN).

The investigated fragments belong to some ancient Roman pipes (called *tibiae*) now stored in the deposits of the MANN. The *tibia*, similar to the Greek *aulos*, was a very popular musical instrument in ancient Rome used in several contexts, especially outdoors. It was a pipe with finger holes and a double reed mouthpiece and was almost always played in pairs. The instrument could be crafted from wood, bone, and/or metal. In the examples found in Pompeii, the instruments are made by bone or wood conjoined segments with a cylindrical internal cavity, and they are covered externally by two metal sheets (also including rotating sleeves, which were mechanisms used by the players to modulate between keys), potentially filled with plant fibers as a filler. Differences in the number of holes and sliding mechanisms had an impact on the types of melodies that could

be produced since, by covering and reopening specific fingerholes, the player could modify the length of the vibrating air column within the pipe and hence produce different notes [1]. An example of a *tibia* is reported in Figure 1.



**Figure 1.** Example of a silver *tibia*, inventory number 76891, stored in the National Archaeological Museum of Naples; image courtesy of the Museum.

Materials composed of metal alloys from archaeological excavation sites are subject to significant corrosion phenomena, leading to the formation of a complex mineralogical stratified layer called “patina” [2–4]. Numerous factors contribute to the initiation of alteration and degradation processes, encompassing the chemical characteristics of the environment, the technological aspects of the artifact, and the presence of biological communities. Consequently, transformations of the chemical composition of the surface alloy occur, leading to the formation of diverse corrosion patinas on the surface.

Nord et al. [5] conducted a comprehensive study on several bronze objects from different archaeological sites in Sweden, focusing on the chemical composition and corrosion products in relation to excavation contexts. Cuprite  $\text{Cu}_2\text{O}$  resulted as the predominant corrosion product among the observed compounds. Malachite  $\text{CuCO}_3\text{Cu}(\text{OH})_2$  and brochantite  $\text{Cu}_4[(\text{OH})_6 | \text{SO}_4]$  were also common; atacamite  $\text{Cu}_2\text{Cl}(\text{OH})_2$  and paratacamite  $\text{Cu}_2[(\text{OH})_3 | \text{Cl}]$  were frequently occurring on bronze objects from soils rich in chlorides. Cornetite  $\text{Cu}_3(\text{PO}_4)(\text{OH})_3$  and other copper phosphates were observed on metal artifacts recovered from graves where the interaction between deteriorated bone and the metal had occurred. The presence of cerussite  $\text{Pb}_3(\text{CO}_3)_2(\text{OH})_2$  indicates a significant amount of Pb in the objects. Other corrosion products, due to water-soluble salts in the soil, were observed. Correspondingly, soil analysis from the artifact’s originating sites revealed that objects from sandy and porous soils are more susceptible to corrosion. Conversely, artifacts from marshy environments with lower oxygen concentrations exhibit better preservation. Soils with acidic pH and a high salt component demonstrate strong corrosive action. The presence of soot in soil aggravates corrosion facilitating a reduction in oxygen [6]. Consequently, total burial time is not the primary factor influencing degradation; rather, it depends on conservation conditions and soil characteristics.

Ingo et al. [2] investigated corrosion layers of artifacts from archaeological contexts, revealing the presence of uncommon patinas. Notably, pyromorphite ( $\text{Pb}_5(\text{PO}_4)_3\text{Cl}$ ), a yellow-green lead chlorophosphate complex, was identified on coins from the Tharros site in Sardinia. This patina’s formation is attributed to the high phosphate percentage in the excavation soil, resulting from decomposing bone fragments.

Phosphate-based corrosion products were also identified by Fan et al. [7], who investigated corrosion products on bronze artifacts from different tombs at the Yujiaba site in China. Beyond the common patinas on copper-based alloys, the presence of phosphates, like libethenite ( $\text{Cu}_2\text{PO}_4(\text{OH})$ ), cornetite ( $\text{Cu}_3\text{PO}_4(\text{OH})_3$ ), and reichenbachite ( $\text{Cu}_5(\text{OH})_4(\text{PO}_4)_2$ ), was ascribed to the influence of the storage environment that was rich in graves and human bones.

Considering the specific context of Pompeii excavations, Pronti et al. [8] focused on the corrosion products of Greek and Roman coins. The influence of volcanogenic salts and their impact on the conservation of metal artifacts have, however, not yet been fully disclosed. Analyzing artifacts from the same excavation campaign and stratigraphic unit, the research identified corrosion patinas, showcasing variations even among artifacts of the

same type due to micro-conditions in the excavation soil. Investigations on fifteen ancient copper-based coins highlighted the presence of several corrosion products. The coins were made of leaded bronzes (Cu, Sn, and Pb), and the analyses showed the presence of cuprite  $\text{Cu}_2\text{O}$ , adjacent to the metal. Malachite  $\text{CuCO}_3\text{Cu}(\text{OH})_2$  and azurite  $2\text{CuCO}_3(\text{OH})_2$  were also found, and both usually grow over the cuprite patina. Cu-Cl-based corrosion products, like nantokite  $\text{CuCl}$ , atacamite  $\text{Cu}_2\text{Cl}(\text{OH})_2$ , and paratacamite  $\text{Cu}_2[(\text{OH})_3|\text{Cl}]$ , were identified. Amorphous tin dioxide was revealed. Cerussite  $\text{Pb}_3(\text{CO}_3)_2(\text{OH})_2$ , plumbonacrite  $\text{Pb}_5(\text{CO}_3)_3\text{O}(\text{OH})_2$ , and plattnerite  $\text{PbO}_2$ , lead-based corrosion products, were observed. Diaboleite  $\text{Pb}_2\text{CuCl}_2(\text{OH})_4$ , an uncommon corrosion product, was detected on a coin.

The present work focused on seven metal fragments belonging to pipes preserved in the storage of the National Archaeological Museum of Naples (MANN), excavated between the 18th and 19th centuries in Pompeii. The primary objectives of this specific project were to identify the composition of the alloys, explore the manufacturing techniques employed in crafting Roman *tibiae*, and assess the presence of surface decoration or ancient protective treatments. Finally, the work also aimed at investigating the corrosion processes affecting *tibiae*, which are peculiar composite (metal/bone) artifacts.

## 2. Materials and Methods

The fragments studied in this research (Table 1) were collected from the boxes in which the flutes are stored; they were already detached from the original artifacts. Because of this, it was not possible to assign the fragments analyzed to their belonging pipes.

**Table 1.** List of investigated *tibiae* samples with Museum information.

Name	Museum Box	Museum Description	Dimensions
AN2	35	Metal	~8.3 × 6.8 × 1.1 mm
AN3		Metal pipe	~4.7 × 5.6 × 0.4 mm
AN4	8/shelf 2	Bronze	~5.4 × 3.9 × 1.0 mm
AN6		Metal pipe	~4.7 × 3.2 × 0.3 mm
AN7	35	Metal pipe	~4.5 × 4.3 × 0.6 mm
AN8	35	Bronze	~10.6 × 6.9 × 0.7 mm
AN11	8/shelf 5 (on the ground)	Metal	~4.5 × 3.5 × 0.5 mm

The initial step consisted of a surface examination of the fragments by a 3D-digital optical microscope (OM), a HIROX HK7700 stereo, equipped with an MX-5040RZ lens (Hirox, Limonest, France). This preliminary observation allowed us to analyze the morphology of the patina layers and gain an initial insight into the diversity of corrosion products. Chemical analysis of corrosion patinas on various fragment sites was performed by Raman investigation through Renishaw Raman InVia spectroscopy with a laser source based on Ar<sup>+</sup> (514.5 nm, P<sub>max</sub> = 30 mW). The excitation power was approximately 0.3–1.5 mW at the sample, and an edge filter monochromator with 1800 lines/mm was used. To optimize the signal-to-noise ratio, each individual scan's time was set to 10 s, with an acquisition number between 2 and 4. The instrument was interfaced with a Leica DMLM optical microscope (Wetzlar, Germany) (objective lenses: 5×, 20×, 50×, 50 × LD), and the detector employed was a thermoelectrically cooled CCD (Charge-Coupled Device) type (203 K). The investigation of organic substances on the sample surfaces was conducted using infrared spectrophotometry with the Bruker Alpha instrument using ATR mode with a diamond crystal in the spectral range of 4000–400 cm<sup>-1</sup>. To identify metal alloys, the fragments' cross-sections (CS) were analyzed by a scanning electron microscope (SEM) with an energy dispersive X-ray spectroscopy (EDS) probe (Zeiss EP EVO 50 (Oberkochen, Germany) with Variable Pressure (VP) set at 100 Pa, equipped with Oxford Instruments' INCA X-act Penta FET<sup>®</sup> Abingdon, Oxfordshire, UK Precision EDS probe). Alloy composition was averaged over at least 4 measurements, and the results are presented with standard deviations. Localized EDS analyses were repeated at least twice in each point, and the average results are presented with standard deviations. Cross-sections, prepared

by conventional metallographic techniques, were observed using the Zeiss Axio Imager A1m and the Reichert-Jung MeF3A optical microscopes (Depew, NY, USA).

### 3. Results

#### 3.1. Identification of Metal Alloys

Through SEM/EDS analysis, the metal alloys used for the *tibia* fragments were identified. The results showed that fragments can be categorized into two distinct groups based on the alloy compositions. Specifically, AN2, AN7, AN8, and AN11 were identified as fragments from brass instruments, whereas AN3, AN4, and AN6 were associated with bronze instruments.

##### 3.1.1. Brass Fragments

AN2, AN7, AN8, and AN11 represent the best-preserved fragments, where, even upon cross-sectional observation, areas with well-preserved metal are discernible (Figure 2).

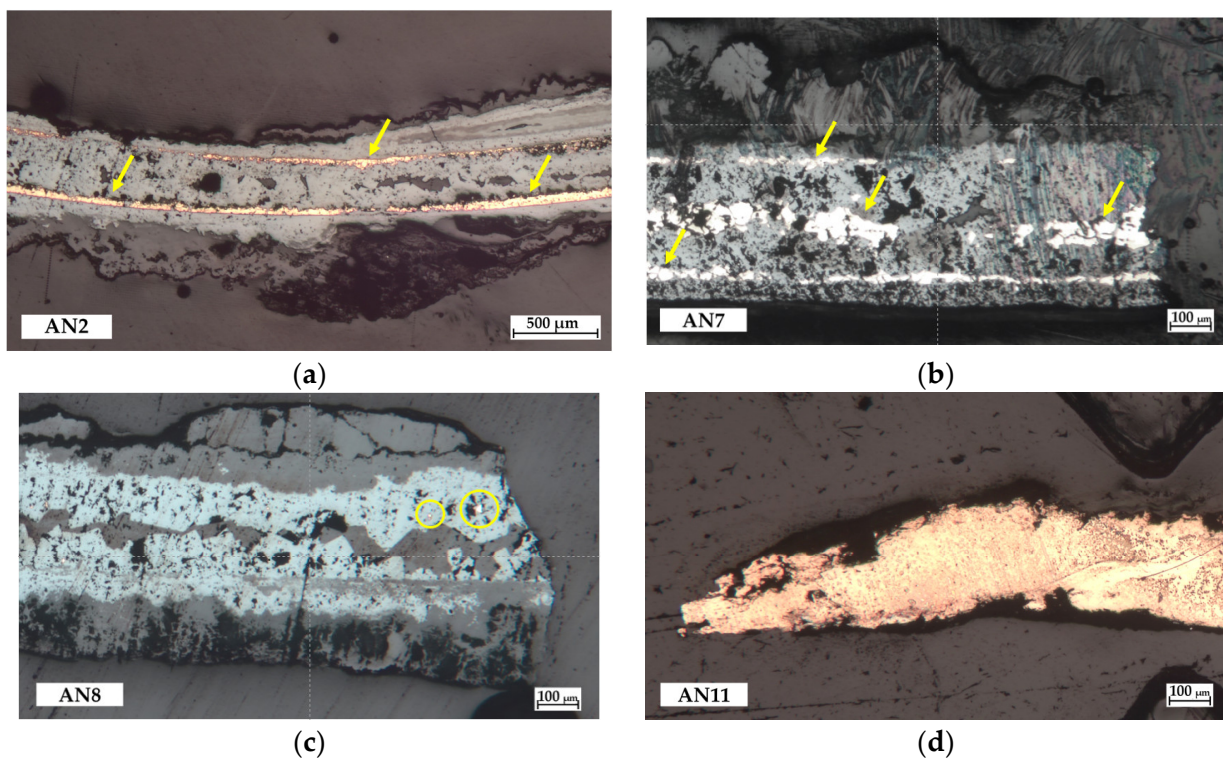


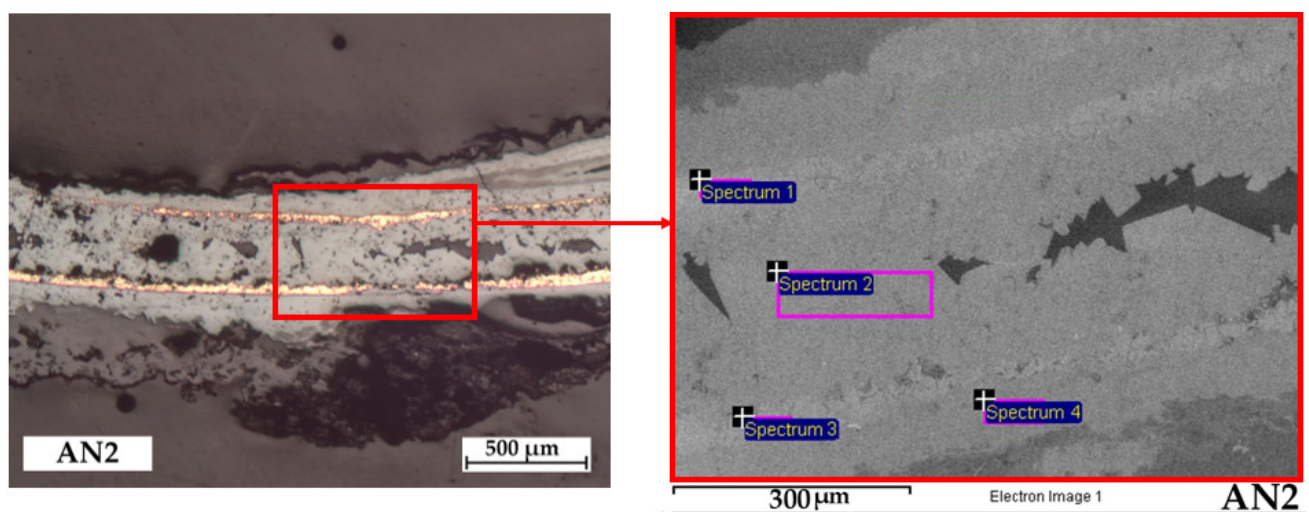
**Figure 2.** Optical images of the cross-section (unetched brass fragments): (a) AN2; (b) AN7; (c) AN8; (d) AN11. The yellow arrows and the yellow circles highlight the areas where the alloy is still preserved.

EDS analysis revealed that these fragments belong to instruments crafted from a brass alloy with an average composition of Cu (approximately 79 wt.%) and Zn (about 11 wt.%) in the metal core (Table 2), with Zn well below the conventional limit of 28 wt.%, above which brass should be regarded with suspicion [9]. Brass is typically composed of Cu and Zn, with Cu being the primary component. In addition to Cu and Zn, other elements, such as Sn and Pb, may also be added to brass alloys to optimize physical and chemical properties [10]. In these fragments, small amounts of Sn (approximately 0.2%) and Pb (average 0.1%) were detected.

**Table 2.** Metal composition of brass fragments in weight%.

	O		S		Si		Cl		Fe		Cu		Zn		Sn		Pb	
	wt%	SD	wt%	SD	wt%	SD	wt%	SD	wt%	SD	wt%	SD	wt%	SD	wt%	SD	wt%	SD
AN2	9.9	1.0	0.1	0.0	-	-	0.2	0.0	-	-	79.7	1.1	9.5	1.66	0.5	0.1	-	-
AN7	9.5	1.65	1.4	1.4	-	-	-	-	-	-	77.9	3.4	10.7	2.2	0.2	0.2	0.1	0.1
AN8	12.2	0.7	0.3	0.1	-	-	0.0	0.1	0.1	0.1	79.1	1.4	8.3	1.1	-	-	-	-
AN11	4.8	0.2	0.0	-	0.3	0.1	0.3	0.0	-	-	78.5	0.4	15.6	0.1	0.2	0.1	0.2	0.1

Optical microscopic observation of the cross-sections of AN2 (Figure 2a) and AN7 (Figure 2b) revealed thin external layers where the alloy is still preserved. Also, SEM/EDS analysis indicated that the inner part of the fragments is mineralized, while the external areas with a bright metallic appearance showed a high percentage of Cu and Zn, indicating the preservation of the alloy (Figure 3, Table 3).

**Figure 3.** SEM-EDS image of the cross-section of AN2 (brass fragments). Pink boxes, corresponding to the spectra 1–5 showed in Table 3, correspond to analysed areas of AN2 cross-section.**Table 3.** Elemental composition of the AN2 cross-section (weight%).

	O		S		Cl		Cu		Zn		Sn	
	wt%	SD	wt%	SD	wt%	SD	wt%	SD	wt%	SD	wt%	SD
Spectrum 1	20.4	12.8	0.2	0.0	0.3	0.2	70.8	13.4	8.0	0.7	0.4	0.2
Spectrum 2	15.5	0.2	0.1	0.0	0.2	0.0	82.4	0.3	1.0	0.0	0.7	0.1
Spectrum 3	19.5	14.2	0.2	0.1	0.3	0.1	71.0	14.0	8.7	0.3	0.3	0.1
Spectrum 4	30.5	17.4	0.2	0.1	0.5	0.2	66.5	16.5	2.0	0.1	0.3	0.2

In contrast, the whole thickness of AN11 is excellently preserved and the brass contained about 15 wt.% Zn. Chemical etching with  $\text{FeCl}_3/\text{HCl}$  showed a recrystallized structure throughout the entire sample thickness, with the presence of several slip bands. This microstructure indicates a final cold working step after hot working (Figure 4) [11].

Lastly, AN8 exhibits a lower percentage of Zn (about 8 wt.%) than the other brass fragments and it is highly mineralized (Figure 2c).

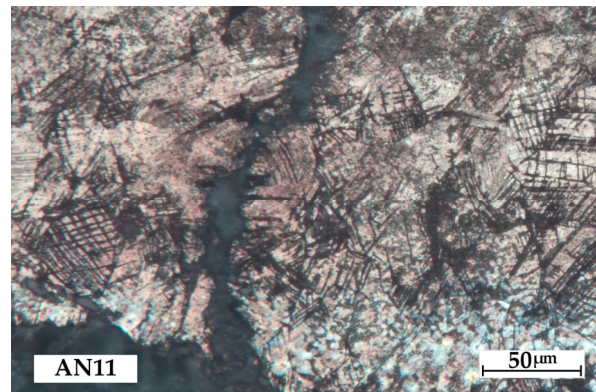


**Figure 4.** AN11 (brass fragment): slip bands highlighted by chemical etching with  $\text{FeCl}_3/\text{HCl}$ .

### 3.1.2. Bronze Fragments

Bronze fragments (AN3, AN4, AN6) exhibit a higher degree of mineralization compared to brass fragments, as no areas were found where the alloy is still preserved in the metallic state. SEM/EDS analysis revealed high percentages of Cu (approximately 68 wt.%) and Sn (about 8 wt.%) in all bronze fragments (Table 4). Nevertheless, SEM/EDS observation of AN3 highlighted a grain structure with slip bands, which is still visible even if mineralized (ghost structure preserved in the corrosion products) and typical of wrought bronze sheet (Figure 5).

**Table 4.** Metal composition of bronze fragments given in weight%.

	O		S		Si		Cl		Cu		Sn		Pb	
	wt%	SD	wt%	SD	wt%	SD	wt%	SD	wt%	SD	wt%	SD	wt%	SD
AN3	26.1	1.52	0.2	0.1	-	-	1.1	0.4	63.0	1.8	9.5	0.67	-	-
AN4	20.1	2.4	-	-	0.3	0.1	0.4	0.0	74.1	4.0	4.7	1.5	0.4	0.0
AN6	20.6	0.1	0.2	0.2	-	-	0.3	0.0	67.9	0.8	11.0	1.5	-	-

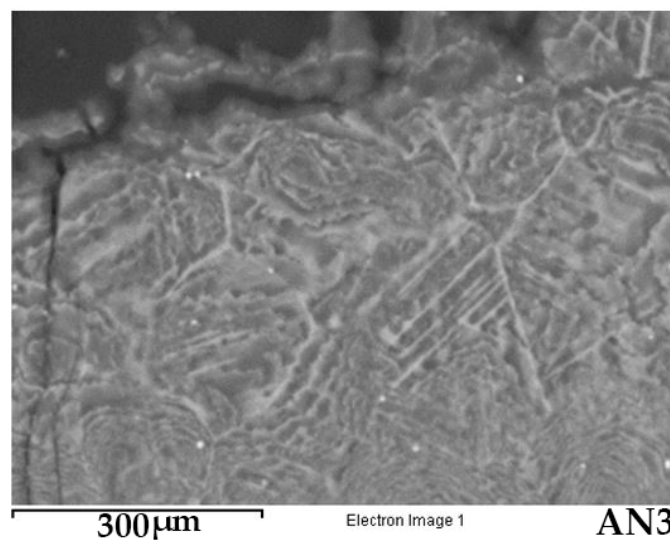


**Figure 5.** AN3 mineralized grain structure.

### 3.1.3. Additional Information Based on Elemental Composition

SEM/EDS investigations gave additional elemental information, contributing to a better understanding of the *tibiae* fragments (Figures 6–9).

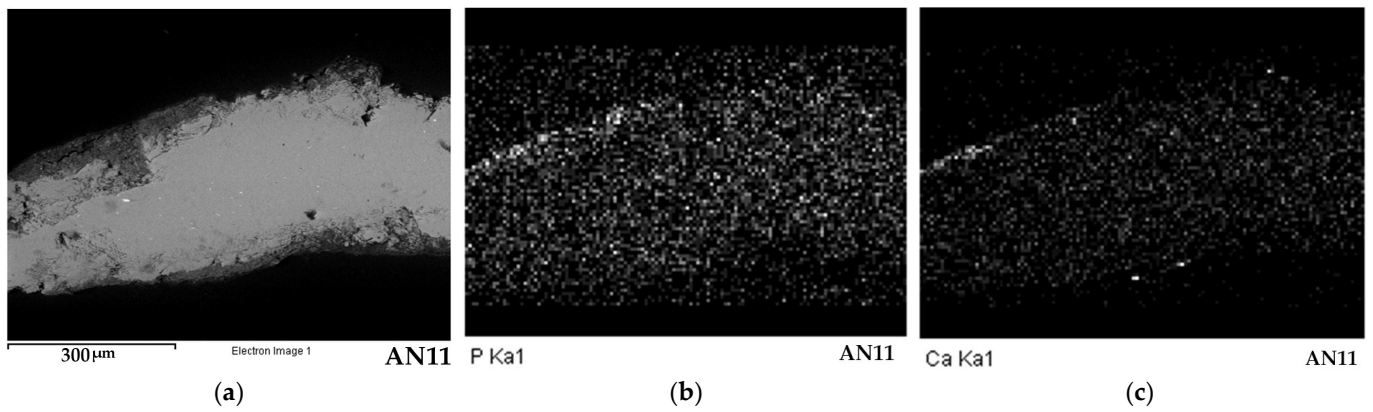


**Figure 6.** Other elements identified through SEM/EDS analysis on AN11: (a) backscattered electron image; (b) P; (c) Ca.

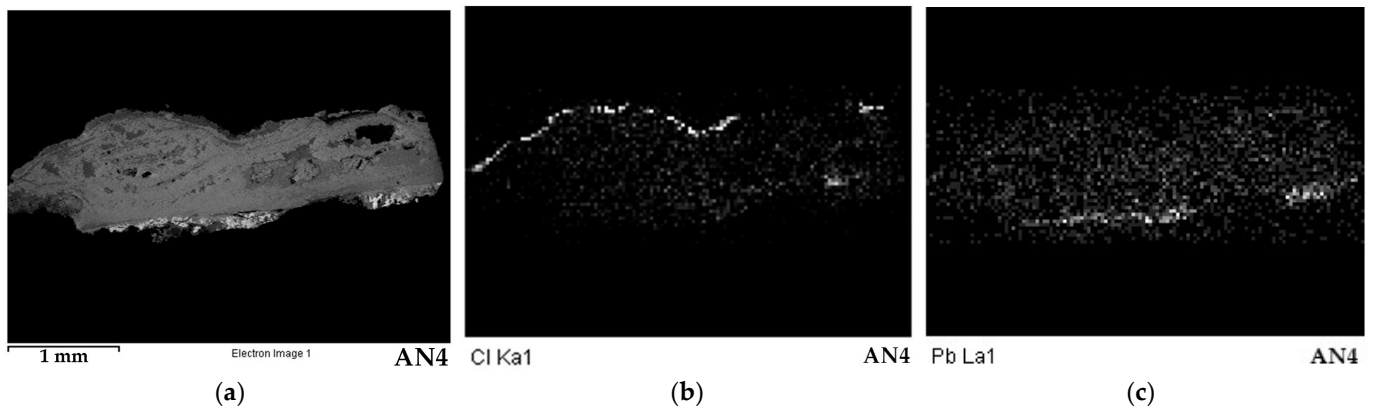


**Figure 7.** Other elements identified through SEM/EDS analysis on AN4: (a) backscattered electron image; (b) Cl; (c) Pb.

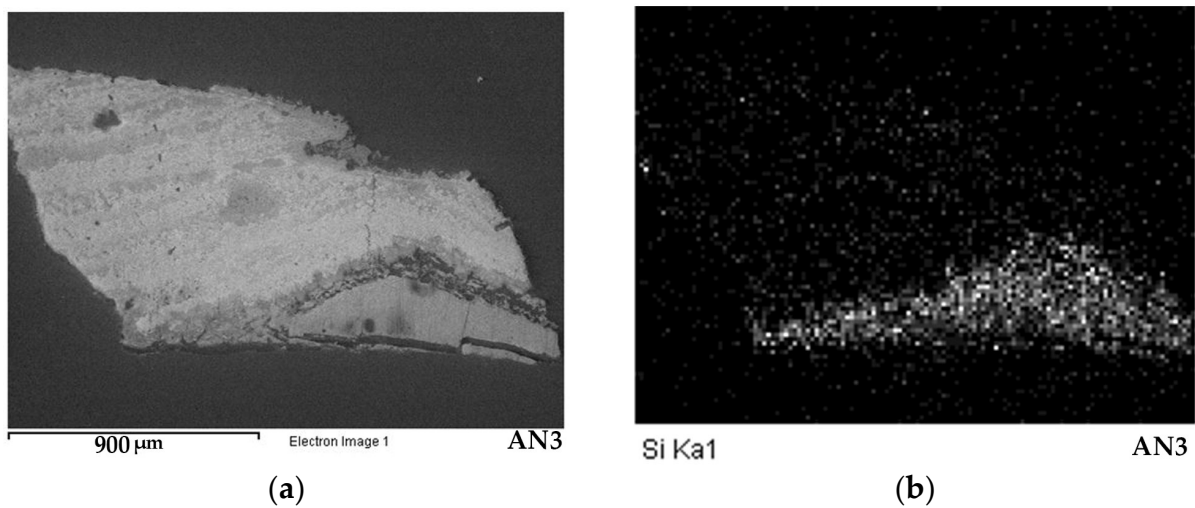


**Figure 8.** Silicon identified through SEM/EDS analysis on AN3: (a) backscattered electron image; (b) Si.

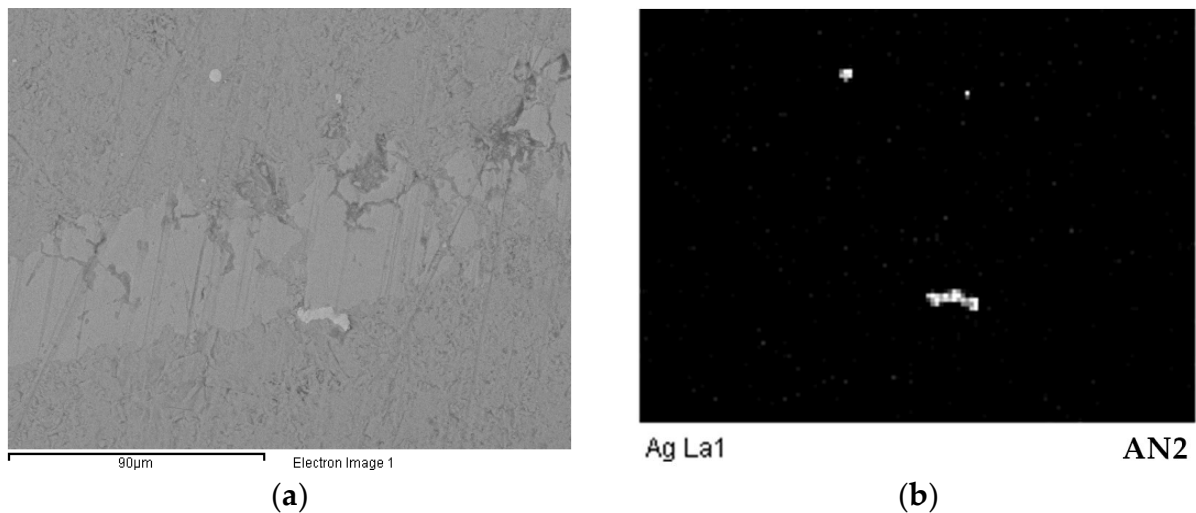


**Figure 9.** Silver identified through SEM/EDS analysis on AN2: (a) backscattered electron image; (b) Ag.

- Phosphorous (P): EDS analysis indicated the presence of P on the inner side of fragment AN11, as depicted in Figure 6b. This observation is likely attributable to the contact with the bones employed in the construction of the *tibia*. The interaction between the metal artifact and bone components led to the accumulation of phosphorus [4,5];
- Calcium (Ca): Traces of this element were detected in fragment AN11 (Figure 6c). They could be attributed, like P, to contact with bone material used in the construction of the tibiae or it could derive from the soil.
- Chlorine (Cl): A notable concentration of Cl was detected on the external side of fragments AN2 and AN11. The same element was detected also on the inner side of AN3 and AN4 (Figure 7b). The presence of Cl suggests a correlation with the excavation soil type, potentially characterized by an abundance of soluble salts, which could stem from proximity to the sea [5] or be derived from volcanic-origin pyroclasts rich in ions [12];
- Lead (Pb): The outer side of fragment AN4 exhibits Pb accumulation, as illustrated in Figure 7c. The presence and the location of this Pb-rich layer on the outer surface were also confirmed by SEM/EDS analysis carried out on the free surface of AN4, without mounting in resin. Also, an optical microscope examination revealed a compact white layer (i.e., the typical color of Pb-based corrosion products) in this location. A subsequent investigation at the specific site confirmed that this white patina is enriched in Pb;
- Silicon (Si): A remarkable concentration of Si was detected in the outer area of fragment AN3, as illustrated in Figure 8b. The presence of Si is likely attributed to the contact with soil;
- Silver (Ag): This element was detected in fragment AN2 (Figure 9b). From the observation of some pipes preserved at the MANN, it was possible to notice that some of the tibiae were made using both sheets of Cu-based alloys and Ag. It is, therefore, supposed that the Ag particles found on the fragment are attributable to contact with Ag-rich sheets.

### 3.2. Characterization of Corrosion Patinas

Upon optical microscope examination, different corrosion patinas were observed. In general, the fragments exhibited a greater variety of corrosion patinas on the inner side, with the exception of AN6 and AN11. These two fragments displayed a more homogeneous surface on both sides compared to the others. Notably, several fragments featured a visibly glossy surface, including AN4, AN6, AN7, AN8, and AN11. The complete set of Raman and IR analyses is presented in the Supplementary Materials.

### 3.2.1. Raman Microspectroscopy

Surface Raman measurements were carried out on the fragments to characterize the phase composition of corrosion products, as well as other substances, due to interaction with the environment (Table 5).

**Table 5.** Corrosion patinas detected by Raman spectroscopy.

Fragments	Inner									External								
	CUP	AZ	MAL	BRO	POS	CLI	ATA	ROS	AUR	CUP	AZ	MAL	BRO	POS	CLI	ATA	ROS	AUR
AN2	+	+	+	+	+	–	–	–	+	+	–	–	–	–	–	–	+	–
AN3	–	–	+	+	–	–	–	–	–	+	–	+	+	–	+	–	–	–
AN4	+	+	+	–	–	+	–	–	–	–	–	+	–	–	–	+	–	–
AN6	+	–	+	–	–	+	+	–	–	+	+	+	–	–	–	–	–	–
AN7	–	+	+	–	–	–	–	–	+	+	+	–	–	–	–	–	–	+
AN8	+	–	+	–	–	–	–	–	+	+	–	+	–	–	–	–	–	–
AN11	+	+	+	–	–	+	–	–	–	–	–	–	–	–	–	–	–	–

CUP: cuprite; AZ: azurite; MAL: malachite; BRO: brochantite; POS: posnjakite; CLI: clinoatacamite; ATA: atacamite; ROS: rosasite; AUR: aurichalcite.

#### Cu-based corrosion layers

In the corrosion analysis of Cu-based layers, various compounds have been identified, each contributing to the patina formation on the fragments.

**Copper oxide:** Cuprite  $\text{Cu}_2\text{O}$  typically appears as a compact, surface-adhered layer with a tendency towards a dark red color. It was found on all fragments. Cuprite is the initial product formed in the corrosion process of copper-based alloys and generally constitutes the layer most adhered to the alloy surface [10]. The attribution of peaks corresponding to cuprite is supported by the literature [13].

**Copper hydroxide carbonates:** Azurite  $2\text{CuCO}_3(\text{OH})_2$  and malachite  $\text{CuCO}_3\text{Cu}(\text{OH})_2$  have been identified [6,9]. Azurite appears as a blue patina and was found on AN2, AN4, AN6, AN7, and AN11. Malachite, usually light green crystals, was detected on all fragments [14]. Both azurite and malachite are significant compounds found in Cu alloys within burial contexts.

**Copper hydroxide sulphates:** Brochantite  $\text{Cu}_4[(\text{OH})_6|\text{SO}_4]$  and posnjakite  $\text{Cu}_4(\text{SO}_4)(\text{OH})_6(\text{H}_2\text{O})$  were also detected [15]. Brochantite, typically appearing as blue, green, or greenish crystals, was found on the outer side of AN2 and both sides of AN3. Its presence is commonly found in monuments exposed outdoors [10], and it may result from interactions with microorganisms in the soil [16] and the abundance of sulfur-based compounds in the Vesuvius area. Posnjakite was found only on the outer side of AN2.

**Copper chlorides:** Clinoatacamite  $\text{Cu}_2[(\text{OH})_3|\text{Cl}]$  and atacamite  $\text{Cu}_2\text{Cl}(\text{OH})_2$  were identified. Those compounds form due to the presence of chlorides in the soil [2,6]. Clinoatacamite, tending towards blue-green, was detected on the inner side of AN4 and AN11, while atacamite, exhibiting green and blue patina, was identified both on the inner side of AN6 and on the external one of AN4. The diversity of patinas reflects the complex interaction with the surrounding soil.

#### Mixed Cu-Zn corrosion layers

In examining the corroded layers with a mixed composition of Cu and Zn, the presence of copper and zinc hydroxide carbonates has been confirmed.

**Copper and zinc hydroxide carbonates:** Rosasite  $(\text{Cu}, \text{Zn})_2[(\text{OH})_2|\text{CO}_3]$  and aurichalcite  $(\text{Zn}, \text{Cu})_5(\text{CO}_3)_2(\text{OH})_6$  (Figure 9). The occurrence of rosasite on the outer side of AN2 (Figure 10a), manifested as light blue crystals, agrees with findings from studies by Yang et al. [17]. Additionally, aurichalcite, exhibiting a radiating crystal shape with colors ranging from white to light blue-green, has been identified on the inner part of AN2 and AN8, as well as on both sides of AN7 (Figure 10b). The Raman shift analysis further supports the presence of aurichalcite.

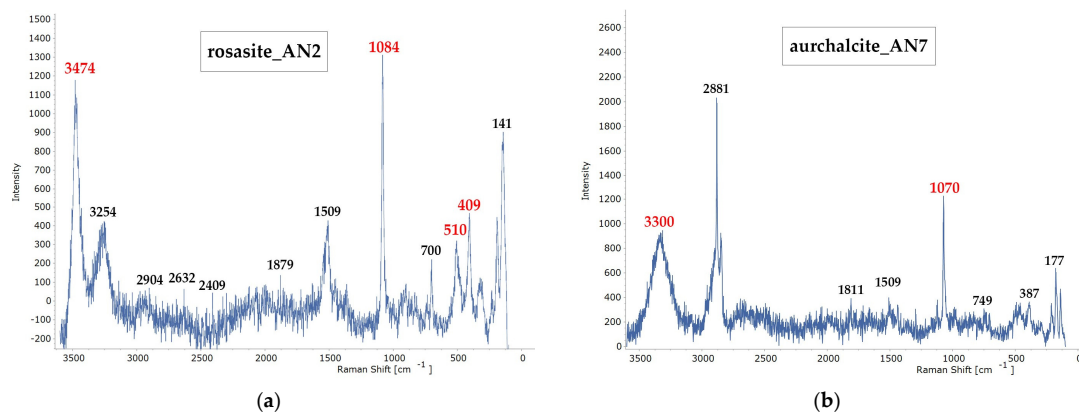


**Figure 10.** Copper and zinc hydroxide carbonates identified through Raman analysis; labels of characteristic peaks of corrosion products are highlighted in red: (a) rosasite on AN2; (b) aurichalcite on AN7.

### 3.2.2. Additional Substances Identified through Raman Analysis

In addition to corrosion products, the following substances listed below were detected:

- Coal: According to the literature [18], peaks indicating the presence of coal were identified on all fragments through Raman analysis, excluding AN4. Coal particles exhibit a dark color, leaning towards black;
- Calcium anhydrous carbonates: Calcite ( $\text{CaCO}_3$ ) was detected on the inner side of AN3 [19]; the fragments AN2 and AN7 also present traces of anhydrous carbonates, either calcite or dolomite  $\text{CaMg}(\text{CO}_3)$ ;
- Anhydrous calcium sulfate: The Raman spectra of gypsum in anhydrous form ( $\text{CaSO}_4$ ) were found in the inner side of the fragment AN4 [20];
- Iron hydroxide: The instrument recorded traces, comparable with the literature [21], of goethite  $\text{Fe}^{+3}\text{O}(\text{OH})$  in the inner side of AN2;
- Lead carbonate: Analysis showed the presence of lead carbonate, hydrocerussite  $\text{Pb}_3(\text{CO}_3)_2(\text{OH})_2$ , on the outer surface of AN4, in correspondence with white areas where Pb was detected by EDS. Raman spectra collected in these areas are comparable to those in the work by Brooker et al. [22];
- Wax: An organic substance of translucent appearance is uniformly present on the surface of the AN3, AN6, AN7, and AN8. In some fragments, traces of the brush strokes of the deposition can still be seen. Through Raman analysis, natural wax peaks were recognized [23];
- “Type 1” substance: An organic layer, distinct from wax, was found on AN4. Raman analysis indicated the presence of carboxyl groups, but the specific material could not be identified;
- “Type 2” substance: The surface of fragment AN11 appears very shiny, suggesting the presence of an overlay. However, Raman analysis did not detect any peaks, precluding the identification of the nature of this layer.

### 3.3. Characterization of Organic Compounds via FTIR

Given the absence of any written reports of conservation interventions on the flutes in the museum archives, it was necessary to carry out additional ATR infrared spectroscopy in order to gain deeper insights into substances that were not identifiable via Raman analysis. This investigation focused exclusively on fragments AN4 and AN11.

In the case of AN4, the spectrum revealed malachite bands. Moreover, a distinctive peak ( $\sim 1735 \text{ cm}^{-1}$ ), characteristic of an ester-type  $\text{C}=\text{O}$  bond, was detected, suggesting the presence of a non-aged siccative oil. In reference to AN11, apart from the malachite bands, peaks corresponding to an ester-type  $\text{C}=\text{O}$  bond were observed. This observation, evident in both the inner and external, hints at the presence of a non-aged siccative oil.

In Table 6, the distribution of organic substances found in the fragments is schematically outlined.

**Table 6.** Organic substances detected by Raman spectroscopy and IR/ATR.

Fragment	Wax	Siccative Oil
AN2	–	+
AN3	+	–
AN4	–	+
AN6	+	–
AN7	+	–
AN8	+	–
AN11	–	+

#### 4. Discussion

The comprehensive analysis of the pipe fragments from Pompeii provides valuable insights into their composition, microstructure, and corrosion processes. In this section, we will discuss each fragment based on the results and data collected.

AN2: The core metal contains about 10 wt.% Zn, suggesting that the sample belongs to an instrument made of brass alloy. A peculiar corrosion stratigraphy was observed: the inner part is completely mineralized, whilst in the outer parts, metallic brass layers are evident. This stratigraphy could result from coating a bronze sheet with brass in order to give the pipe a gilded appearance. The presence of localized Ag particles could be further evidence of surface decorations or application of functional Ag-based coatings. Archaeological findings provide evidence of the use of Ag in crafting certain components of the pipe sheet metal, especially in the case of particularly prestigious musical instruments, such as the so-called “silver pipes” that are also found in Pompeii in 1867 and are quite well-preserved [inv. 76891-4]. The patina on the inner layer of the fragment primarily consists of cuprite (near the interface with the metal core), with a top layer consisting of azurite and malachite. Malachite is the more stable phase and usually grows uniformly on cuprite. This process is caused by the dissolution of copper oxide and the consequent precipitation of copper salts on the surface [4,6]. The presence of Zn in the alloy led to the formation of Zn-containing corrosion patinas, like aurichalcite and rosasite. Aurichalcite is one of the first products of corrosion during the aging of Zn and Cu alloys [24]. Also, brochantite was detected in the outermost part of this patina, along with a small amount of posnjakite. Their location in the patina could result from interaction with the presence of S-based compounds in the Vesuvius area or microorganisms in the soil. Elements and compounds resulting from interaction with soil were detected on both sides of the fragment: Cl on the external side, goethite and anhydrous calcium carbonates in the inner part, and coal residues on both sides.

AN3: The sample is highly mineralized and there is no evidence of the preserved alloy. The absence of Zn and the state of preservation suggest that this fragment belongs to a bronze instrument. The grain structure was recrystallized with slip bands and was still discernible even though it was mineralized, which is characteristic of a wrought bronze sheet. Several corrosion products commonly found in the Cu-based alloys were detected on this fragment. A corrosion patina was composed of cuprite, malachite, atacamite, and brochantite. The presence of atacamite is confirmed by the presence of Cl on the sample. This may be due to the type of excavation soil, which is rich in soluble salts. The interaction with the soil also led to the presence of traces of silicon, calcite, and coal on the surface of the fragment. The waxy substance found on the surface is attributed to protective treatments applied after excavation, in recent times.

AN4: The sample is highly mineralized and there is no evidence of the preserved alloy. The core metal contains Cu and Sn, suggesting that the sample belongs to a bronze instrument. The corrosion patina is composed of cuprite, azurite, malachite, atacamite, and clinoatacamite. Atacamite can convert into clinoatacamite, which is more stable [25]. The interaction with S-based species resulted in the formation of copper hydroxide sulfates, such as brochantite and posnjakite. Pb accumulation in the form of a layer about 60 µm thick is evident on the outer side of the sample, with the presence of hydrocerussite  $Pb_3(CO_3)_2(OH)_2$  and plumbonacrite  $Pb_5(CO_3)_3O(OH)_2$ . Pb may derive from the ternary

composition of the original bronze alloy (comprising Cu, Sn, and Pb), or it could result from an overlying layer applied through decoration techniques. The first hypothesis appears less plausible, as the concentration of Pb is confined to the external of the sample. This suggests that the presence of a Pb-rich layer may be related to a manufacturing technique, such as soldering residues. The presence of gypsum in anhydrous form ( $\text{CaSO}_4$ ) is related to the inorganic components of the soil. A substance with an ester-type  $\text{C}=\text{O}$ , maybe related to non-aged siccative oils, could be due to a restoration treatment [26].

AN6: The sample is highly mineralized; the presence of Sn (about 11 wt.%) suggests that the sample belongs to a bronze instrument. Cuprite, azurite, malachite, atacamite, and clinoatacamite were detected on the surface, together with coal and wax.

AN7: The state of preservation and the type of corrosion products are similar to AN2. The metal core contains about 10% Zn, suggesting that the sample belongs to an instrument consisting of a brass alloy. Mineralized layers of cuprite alternate with layers in which the brass alloy is still preserved in the metallic state. This peculiar stratigraphy could suggest the presence of two alloys, maybe referring to a manufacturing technique where a bronze alloy was covered with a brass layer to achieve a gold-like coloration. Alternatively, it could also result from the dezincification process of brass, followed by the precipitation of a metallic layer due to a modification of exposure conditions [27], generating a reducing environment, which may have occurred as a consequence of the sudden covering by volcanic debris. The corrosion patina consists of cuprite, azurite, malachite, and aurichalcite. Moreover, Zn in the alloy led to the formation of Zn-containing corrosion patinas. Aurichalcite crystals have an acicular shape and are well formed, probably by a slow crystallization process. Anhydrous calcium carbonates were likely due to the contact with the soil; coal and wax were identified on both sides of the sample.

AN8: The metal core contains a lower percentage of Zn (about 8%) than the other brasses and is highly mineralized, except for some metallic grains. The presence of Zn suggests that the sample belongs to a brass instrument. Unlike AN2 and AN7, AN8 does not show any particular stratigraphy. The metal core is largely mineralized and mostly consists of cuprite. Moving from the core towards the external surface, malachite, brochantite, aurichalcite, and azurite were detected. Azurite composed the last layer of the patina and was formed on top of aurichalcite crystals. Coal and wax were identified on both sides of the sample.

AN11 is the best-preserved (i.e., more metallic) fragment. It contains about 15% Zn, suggesting that the sample belongs to an instrument consisting of a brass alloy. The corrosion products consist of cuprite, azurite, malachite, and clinoatacamite. Phosphorus and calcium, probably attributable to contact with the bones used in the construction of the *tibia*, are observed on the inner side of the sheet. The good preservation state of this fragment allowed us to observe its microstructure. Corrosion and chemical etching highlight recrystallized grains, with slip bands and cracks due to deep work hardening. Like AN4, the surface is covered with an ester-type substance, likely related to non-aged siccative oils.

## 5. Conclusions

This study of seven metal fragments attributed to Roman pipes from the archaeological site of Pompeii and preserved in the deposit of the National Archaeological Museum of Naples contributes to knowledge on ancient musical instruments crafting and the study of degradation and alteration processes of metallic artifacts in archaeological contexts. The achieved results can be described as follows.

Identification of metal alloys and manufacturing technologies: Two types of copper-based alloys used for crafting were identified: brass (AN2, AN7, AN8, AN11) and bronze (AN3, AN4, AN6), in the form of wrought sheets. The preservation status of fragments significantly differs between the two alloys, with brass-containing fragments exhibiting better preservation compared to completely mineralized bronze ones. The peculiar stratigraphy observed in AN2 and AN7, characterized by a fully mineralized core and external brass

layers, suggests the application of brass foils to cover the bronze core so as to simulate a gold-like coloration. Traces of silver may be attributable to contact with silver sheets used in *tibiae* manufacturing, which may have induced galvanic coupling, hence stimulating corrosion of the bronze substrate, which is completely mineralized. The Pb-rich layer on the external side of AN4 could be associated with residues from soldering, whilst P and Ca in the inner side of AN11 could be attributable to contact with the bones used in the manufacturing of the pipe.

**Corrosion patina and interaction with burial soil:** The unique environmental conditions of Pompeii, resulting from the eruption of Vesuvius in 79 B.C., contributed to the exceptional conservation of archaeological artifacts. The ejected pyroclastic materials “sealed” the site of Pompeii, serving as a protective shield against external sources of deterioration [28]. However, the complete extent of the influence of volcanogenic products and their effects on the preservation of metal artifacts remains to be fully understood. The interaction with the excavation soil and its chemical composition contributed to the formation of complex patinas on the surface of the samples. Coal particles, attributed to soot, are present on all fragments, except AN4. Iron oxides, calcium carbonates, and anhydrous calcium sulfates are also traced back to soil composition. Indeed, the fragments are characterized by some of the typical corrosion products found on metallic artifacts preserved in archaeological contexts, such as cuprite, azurite, malachite, atacamite, and clinoatacamite; brochantite and posnjakite, generally found on metal artifacts exposed outdoors, were also detected. The patina of the brass fragments is also characterized by aurichalcite and rosasite and Cu and Zn hydroxide carbonates.

**Conservative superficial treatments:** The identification of organic substances, like wax and siccative oil, on the surface suggests potential surface treatments. The origin of these substances, whether ancient or more recent applications post-excavation, remains uncertain.

This study represents a preliminary investigation into the materials and manufacturing techniques employed in the production of *tibiae* instruments. Further analyses are planned to gain a more comprehensive understanding of these instruments.

**Supplementary Materials:** The following supporting information can be downloaded at: <https://www.mdpi.com/article/10.3390/heritage7050121/s1>, Figure S1: Cuprite Raman spectrum revealed on AN2 and cuprite standard; Figure S2: Azurite Raman spectrum revealed on AN2 and azurite standard; Figure S3: Malachite Raman spectrum revealed on AN2 and malachite standard; Figure S4: Brochantite Raman spectrum and posnjakite peaks revealed on AN3 and brochantite and posnjakite standard; Figure S5: Clinoatacamite Raman spectrum revealed on AN11 and clinoatacamite standard; Figure S6: Atacamite Raman spectrum revealed on AN4 and atacamite standard; Figure S7: Rosasite Raman spectrum revealed on AN2 and rosasite standard; Figure S8: Aurichalcite Raman spectrum revealed on AN7 and aurichalcite standard; Figure S9: Hydrocerussite Raman spectrum revealed on AN4 and hydrocerussite standard; Figure S10: Wax Raman spectrum revealed on AN3; Figure S11: Wax Raman spectra revealed on AN3; Figure S12: Siccative oil IR spectrum revealed on AN11.

**Author Contributions:** Conceptualization, S.S., C.C., G.F., M.M. (Marco Malagodi), C.M., M.M. (Maria Morisco) and E.R.; methodology, S.S., C.C., G.F., M.M. (Marco Malagodi) and C.M.; validation, M.M. (Maria Morisco); investigation, S.S., C.C. and C.M.; data curation, S.S., C.C. and C.M.; writing—original draft preparation, S.S.; writing—review and editing, C.C., G.F., M.M. (Marco Malagodi), C.M. and E.R.; supervision, C.C., C.M., M.M. (Marco Malagodi) and E.R. All authors have read and agreed to the published version of the manuscript.

**Funding:** This research received no external funding.

**Data Availability Statement:** The raw data supporting the conclusions of this article will be made available by the authors upon request.

**Acknowledgments:** The authors would like to thank the National Archaeological Museum of Naples for providing access to the archaeological artifacts.

**Conflicts of Interest:** The authors declare no conflicts of interest.

## References

1. Hagel, S. Re-evaluating the Pompeii Auloi. *J. Hell. Stud.* **2008**, *128*, 52–71. [[CrossRef](#)]
2. Ingo, G.M.; De Caro, T.; Ricucci, C.; Khosroff, S. Uncommon corrosion phenomena of archaeological bronze alloys. *Appl. Phys. A* **2006**, *83*, 581–588. [[CrossRef](#)]
3. Hassiri, H.; Bousselmi, L.; Triki, E. Bronze degradation processes in simulating archaeological soil media. *J. Solid State Electrochem.* **2010**, *14*, 393–401. [[CrossRef](#)]
4. Doménech-Carbò, A.; Doménech-Carbò, M.T.; Martínez-Làzaro, I. Electrochemical identification of bronze corrosion products in archaeological artefacts. A case study. *Microchim. Acta* **2008**, *162*, 351–359. [[CrossRef](#)]
5. Nord, A.G.; Mattsson, E.; Tronner, K. Factors Influencing the Long-term Corrosion of Bronze Artefacts in Soil. *Prot. Met.* **2005**, *41*, 309–316. [[CrossRef](#)]
6. Mattsson, E. *Basic Corrosion Technology for Scientists and Engineers*, 2nd ed.; CRC Press: London, UK, 1999.
7. Fan, X.; Wang, Q.; Wang, Y. Non-destructive in situ Raman spectroscopic investigation of corrosion products on the bronze dagger-axes from Yujiaba site in Chongqing, China. *Archaeol. Anthr. Sci.* **2020**, *12*, 90. [[CrossRef](#)]
8. Pronti, L.; Felici, A.C.; Alesiani, M.; Tarquini, O.; Bracciale, M.P.; Santarelli, M.L.; Pardini, G.; Piacentini, M. Characterisation of corrosion layers formed under burial environment of copper-based Greek and Roman coins from Pompeii. *Appl. Phys. A* **2015**, *121*, 59–68. [[CrossRef](#)]
9. Craddock, P.T. *Scientific Investigation of Copies, Fakes and Forgeries*; Butterworth-Heinemann Elsevier Ltd.: Oxford, UK, 2009.
10. Scott, D.A. *Copper and Bronze in Art: Corrosion, Colorant, Conservation*; The Getty Conservation Institute; Getty Publications: Los Angeles, CA, USA, 2002.
11. Caron, R.N.; Barth, R.G.; Tyler, D.E. Metallography and Microstructures of Copper and Its Alloys. In *Metallography and Microstructures*; Voort, G.F.V., Ed.; ASM Handbook; ASM International: Materials Park, OH, USA, 2004; Volume 9, ISBN 978-1-62708-177-1. [[CrossRef](#)]
12. Balcone-Boissard, H.; Villemant, B.; Boudon, G.; Michel, A. Non-volatile vs volatile behaviours of halogens during the AD 79 plinian eruption of Mt. Vesuvius, Italy. *Earth Planet. Sci. Lett.* **2008**, *269*, 66–79. [[CrossRef](#)]
13. De Caro, T.; Angelini, E.; Es Sebar, L. Application of m-Raman spectroscopy to the study of the corrosion products of archaeological coins. *Acta IMEKO* **2021**, *10*, 234–240. [[CrossRef](#)]
14. Fu, Q.; Pu-jun, J.; Xue, L.; Shang-xin, Z.; Wei-gang, S.; Yin, X. Preliminary Study of Corrosion Status on Bronzes Excavated from Qin Dynasty Tombs at Xinfeng Town in China. *Int. J. Corros.* **2012**, *2012*, 150380. [[CrossRef](#)]
15. Hayez, V.; Guillaume, J.; Hubin, A.; Terryn, H. Micro-Raman spectroscopy for the study of corrosion products on copper alloys: Setting up of a reference database and studying works of art. *J. Raman Spectrosc.* **2004**, *35*, 732–738. [[CrossRef](#)]
16. Muros, V.; Scott, D.A. The occurrence of brochantite on archaeological bronzes: A case study from Lofkënd, Albania. *Stud. Conserv.* **2016**, *63*, 113–125. [[CrossRef](#)]
17. Yang, J.; Cheng, H.; Frost, L.R. Synthesis and characterisation of cobalt hydroxy carbonate  $\text{Co}_2\text{CO}_3(\text{OH})_2$  nanomaterials. *Spectrochim. Acta A Mol. Biomol. Spectrosc.* **2011**, *78*, 420–428. [[CrossRef](#)] [[PubMed](#)]
18. Potgieter-Vermaak, S.; Maledi, N.; Wagner, N.; Van Heerden, J.H.P.; Van Grieken, R.; Potgieter, J.H. Raman spectroscopy for the analysis of coal: A review. *J. Raman Spectrosc.* **2010**, *42*, 123–129. [[CrossRef](#)]
19. Rutt, H.N.; Nicola, J.H. Raman spectra of carbonates of calcite structure. *J. Phys. C Solid State Phys.* **1974**, *7*, 4522. [[CrossRef](#)]
20. Brotton, S.J.; Kaiser, R.I. In Situ Raman Spectroscopic Study of Gypsum ( $\text{CaSO}_4 \cdot 2\text{H}_2\text{O}$ ) and Epsomite ( $\text{MgSO}_4 \cdot 7\text{H}_2\text{O}$ ) Dehydration Utilizing an Ultrasonic Levitator. *J. Phys. Chem. Lett.* **2013**, *4*, 669–673. [[CrossRef](#)] [[PubMed](#)]
21. De Faira, D.L.A.; Lopes, F.N. Heated goethite and natural hematite: Can Raman spectroscopy be used to differentiate them? *Vib. Spectrosc.* **2007**, *45*, 117–121. [[CrossRef](#)]
22. Brooker, M.H.; Sunder, S.; Taylor, P.; Lopata, V.J. Infrared and Raman spectra and X-ray diffraction studies of solid lead(II) carbonates. *Can. J. Chem.* **1983**, *61*, 494–502. [[CrossRef](#)]
23. Bergamonti, L.; Cirilini, M.; Graiff, C.; Lottici, P.P.; Palla, G.; Casoli, A. Characterization of Waxes in the Roman Wall Paintings of the Herculaneum Site (Italy). *Appl. Sci.* **2022**, *12*, 11264. [[CrossRef](#)]
24. Spencer, M.S. The role of zinc oxide in Cu/ZnO catalysts for methanol synthesis and the water–gas shift reaction. *Top. Catal.* **1999**, *8*, 259–266. [[CrossRef](#)]
25. Jambor, J.L.; Dutrizac, J.E.; Roberts, A.C.; Grice, D.J.; Szymanski, J.T. Clinoatacamite, a new polymorph of  $\text{Cu}_2(\text{OH})_3\text{Cl}$ , and its relationship to paratacamite and “Anarakite”. *Can. Mineral.* **1996**, *34*, 61–72.
26. Risser, E.; Saunders, D. (Eds.) *The Restoration of Ancient Bronzes: Naples and Beyond*; Los Angeles Getty Publications Virtual Library; Getty Publications: Los Angeles, CA, USA, 2013.
27. Scott, D.A. Periodic Corrosion Phenomena in Bronze Antiquities. *Stud. Conserv.* **1985**, *30*, 49–57. [[CrossRef](#)]
28. Pérez-Diez, S.; Fernández-Menéndez, L.J.; Morillas, H.; Martellone, A.; De Nigris, B.; Osanna, M.; Bordel, N.; Caruso, F.; Madariaga, J.M.; Maguregui, M. Elucidation of the Chemical Role of the Pyroclastic Materials on the State of Conservation of Mural Paintings from Pompeii. *Angew. Int. Ed. Chem.* **2021**, *133*, 3065–3073. [[CrossRef](#)] [[PubMed](#)]

**Disclaimer/Publisher’s Note:** The statements, opinions and data contained in all publications are solely those of the individual author(s) and contributor(s) and not of MDPI and/or the editor(s). MDPI and/or the editor(s) disclaim responsibility for any injury to people or property resulting from any ideas, methods, instructions or products referred to in the content.